Bioactive Materials 6 (2021) 2250–2260

Contents lists available at ScienceDirect

Bioactive Materials

journal homepage: www.sciencedirect.com/journal/bioactive-materials

Biomimetic mineralized hybrid scaffolds with antimicrobial peptides

Zhou Ye [b,1], Xiao Zhu [a,1], Isha Mutreja [b], Sunil Kumar Boda [b], Nicholas G. Fischer [b], Anqi Zhang [b], Christine Lui [b], Yipin Qi [c], Conrado Aparicio [b,*]

[a] The State Key Laboratory Breeding Base of Basic Science of Stomatology & Key Laboratory of Oral Biomedicine Ministry of Education, School of Stomatology, Wuhan University, Wuhan, 430079, China

[b] Minnesota Dental Research Center for Biomaterials and Biomechanics, Department of Restorative Sciences, School of Dentistry, University of Minnesota, MN, 55455, USA

[c] Department of Operative Dentistry and Endodontics, Guanghua School of Stomatology, Hospital of Stomatology, Guangdong Key Laboratory of Stomatology, Sun Yat-sen University, Guangzhou, 510000, China

ARTICLE INFO

Keywords:
Biomimetic mineralization
Antimicrobial
Cationic and amphipathic peptides
Hard tissue
cytocompatibility

ABSTRACT

Infection in hard tissue regeneration is a clinically-relevant challenge. Development of scaffolds with dual function for promoting bone/dental tissue growth and preventing bacterial infections is a critical need in the field. Here we fabricated hybrid scaffolds by intrafibrillar-mineralization of collagen using a biomimetic process and subsequently coating the scaffold with an antimicrobial designer peptide with cationic and amphipathic properties. The highly hydrophilic mineralized collagen scaffolds provided an ideal substrate to form a dense and stable coating of the antimicrobial peptides. The amount of hydroxyapatite in the mineralized fibers modulated the rheological behavior of the scaffolds with no influence on the amount of recruited peptides and the resulting increase in hydrophobicity. The developed scaffolds were potent by contact killing of Gram-negative *Escherichia coli* and Gram-positive *Streptococcus gordonii* as well as cytocompatible to human bone marrow-derived mesenchymal stromal cells. The process of scaffold fabrication is versatile and can be used to control mineral load and/or intrafibrillar-mineralized scaffolds made of other biopolymers.

1. Introduction

Treating bone defects caused by trauma, tumor excision, or pathologic bone resorption can be challenging due to associated risks for infection, particularly for open fractures [1]. Pus that spreads from the infected bone defect region could reduce vascular functions, for example, impairing the exchange of oxygen and nutrients and the recruitment of bone-related cells [2]. Similarly, oral bacterial infection significantly inhibits the regeneration of alveolar bone in periodontitis and peri-implantitis [3]. Bone autografts and allografts or scaffolds made from natural or synthetic materials [4] are often used to promote bone/dental tissue regeneration. However, these materials are also prone to bacterial attachment and could further increase the risk of infection [5].

The conventional treatment modality for infected bone defects includes debridement, removal of implants/scaffolds/biomaterial, and systemic antibiotic therapies [6]. However, the administration of systemic antibiotics is not effective due to the poor blood supply in the infected region [2] and the increasing bacterial resistance to antibiotics. Consequently, it is critical to develop new hard tissue engineering scaffolds with synergistic functions of reducing local bacterial infections and promoting bone regeneration. These scaffolds could be intrinsically antimicrobial or loaded with antibiotics, antimicrobial metallic ions, and/or nanoparticles [7]. Inspired by our previous work in which we applied a stable coating of antimicrobial peptides (AMPs) on dentin to prevent the failure of dental restorations by infection [8,9], here we developed a bioinspired hybrid scaffold composed of bone/dentin-like mineralized collagen nanostructures combined with AMPs.

Bone and dentin are natural biocomposites mainly comprised of collagen and hydroxyapatite (HA). Many methods have been developed to produce collagen-HA composite scaffolds, including immersion of collagen scaffolds in simulated body fluid (SBF) [10], freeze casting of collagen-HA precipitates [11], electrospinning of collagen solution mixed with HA nanoparticles [12], and 3D printing of homogenized

Peer review under responsibility of KeAi Communications Co., Ltd.
* Corresponding author.
E-mail address: apari003@umn.edu (C. Aparicio).
[1] These authors contributed equally.

https://doi.org/10.1016/j.bioactmat.2020.12.029
Received 2 October 2020; Received in revised form 15 December 2020; Accepted 31 December 2020
Available online 22 January 2021

collagen and HA ink [13]. Mineralized collagen fibrils are basic building blocks of bone and dentin, in which the crystal platelets are organized in layers that traverse across collagen fibrils [14]. To mimic the nanostructure of mineralized collagen fibrils, the polymer-induced liquid-precursor (PILP) process [15] uses polyelectrolytes or proteins, such as polyaspartic acid (pAsp), polyacrylic acid (PAA), poly(allylamine) hydrochloride (PAH), carboxymethyl chitosan (CMC) or osteopontin (OPN), to induce the intrafibrillar mineralization of collagen fibrils [16–21]. PILP-mineralized collagen scaffolds have been demonstrated to promote differentiation of preosteoblasts or bone marrow mesenchymal stem cells *in vitro* and accelerate bone regeneration in rodent calvarial bone defects *in vivo* [20,22,23]. PILP can also be used to repair dentin defects [24] or fabricate bone-like models to study bone physiology and disease [19]. However, the multifunctionality of PILP-mineralized collagen scaffolds remains vastly unexplored. Here, we introduced multifunctionality in the scaffolds by combining osteogenic potential, provided by the intrafibrillar minerals in collagen, with antimicrobial potency, provided by the further incorporation of AMPs. In addition, although the PILP process can successfully induce intrafibrillar mineralization, extrafibrillar minerals often coherently form on the surface of collagen fibrils, which inhibit the diffusion of PILP nanoclusters into the inner layers of a thick scaffold [25]. Consequently, most of the scaffolds mineralized by the PILP process are thin films with a thickness of less than a few hundred microns or sponges with thickness of less than 2 mm [16,17,26]. We previously demonstrated that control over PAA molecular weight, concentration of the PILP mineralizing solution, and time of mineralization led to pure intrafibrillar mineralization and thus, fabrication of homogenous mineralized scaffolds through their whole thickness [21].

AMPs are promising antimicrobial candidates that induce lower levels of bacterial resistance than conventional antibiotics [27]. AMP coatings on scaffolds [28,29] or implant surfaces [30,31] can be efficacious against bacterial infections. There are seven AMPs approved by the US Food and Drug Administration that have been clinically used mainly to treat bacterial skin infections [32]. Human cathelicidin LL-37 has also been evaluated in phase II clinical studies to treat venous leg ulcers. Here we coated the mineralized collagen scaffolds with a human salivary protein derived AMP, GL13K, which is potent against a variety of bone and dental related pathogenic bacteria in solution [33] and on coated substrates [9,34,35]. GL13K is cytocompatible against human dental pulp cells and fibroblasts [9] and antimicrobial in human saliva and fetal calf serum [33].

2. Experimental

2.1. Fabrication of collagen gel

Bovine type I collagen solution at 3 mg/mL, 97% purity and pH = 2 was purchased from Advanced BioMatrix, Inc. (PureCol®, San Diego, CA, USA). 3D collagen gel samples were reconstituted as described previously [21]. Briefly, 24 mL of collagen solution was neutralized with 6 ml of 10 × phosphate buffered saline (PBS) and 4 mL of 0.1 N NaOH solution in an ice bath. The mixed solution was loaded into a 96-well plate with 300 μL in each well and incubated at 30 °C for 3 days. Reconstituted collagen gels were carefully transferred to a 48-well plate and cross-linked in a solution of 50 mM 2-(N-morpholino)ethanesulfonic acid hydrate (MES, Sigma-Aldrich, St. Louis, MO, USA) at pH 7 with 50 mM 1-ethyl-3-(3-dimethylaminopropyl)carbodiimide hydrochloride (EDC, Sigma-Aldrich, St. Louis, MO, USA) and 25 mM N-hydroxysuccinimide (NHS, Sigma-Aldrich, St. Louis, MO, USA) overnight. The reaction was quenched in a solution of 0.1 M Na_2HPO_4 and 2 M NaCl for 2 h. The collagen gels were then washed by deionized (DI) water three times and kept in DI water at 4 °C overnight to further remove salts.

2.2. Mineralization of collagen gel

Collagen gels were mineralized using a previously reported solution [21] containing 4.5 mM $CaCl_2$, 2.1 mM K_2HPO_4 and 50 mg/L PAA (Polysciences, Inc., Warrington, PA, USA) of 450 kDa molecular weight (MW) in tris-buffered saline (TBS) at pH 7.4. Using this condition, the collagen fibrils were intrafibrillarly mineralized [21]. The mineralization solution was filtered with 0.2 μm vacuum filters (Thermo Fisher Scientific, Waltham, MA, USA) prior to use. Collagen gels were incubated at 37 °C on a shaker for 1, 2, 4 and 8 days and named "1d-M", "2d-M", "4d-M" and "8d-M". The pristine collagen gel without mineralization was named "0d-M". The mineralization solution was refreshed every two days to exclude possible extrafibrillar growth of minerals. After mineralization, collagen gels were washed three times with DI water and kept in DI water at 4 °C prior to further use.

2.3. Coating of mineralized collagen with GL13K peptides

Antimicrobial GL13K (GKIIKLKASLKLL-NH_2) peptides were purchased from AAPPTec, LLC (Louisville, KY, USA) with purity >98%. A coating solution was prepared by dissolving GL13K in DI water at 1 mM (1.4 mg/mL). Pristine and mineralized collagen gels were immersed for 15 min in 250 μL GL13K coating solution per well in a 48-well plate to obtain hybrid mineralized collagen/antimicrobial peptide samples. After coating, the samples were washed with DI water three times to remove loosely bound GL13K.

2.4. Scanning electron microscopy (SEM)

Pristine (0d-M) and mineralized (1d-M, 2d-M, 4d-M and 8d-M) collagen samples without or with GL13K coating were lyophilized overnight. Lyophilized collagen samples were sputter-coated with a 5 nm thick Iridium layer and imaged using field emission SEM (Hitachi SU8230, Tokyo, Japan) at an accelerating voltage of 3 kV.

2.5. Transmission electron microscopy (TEM)

Lyophilized 8d-M collagen samples were pulverized in liquid nitrogen, dispersed in ethanol, and deposited on a lacey carbon/formvar grid (Ted Pella Inc., Redding, CA, USA). Unstained samples were imaged using TEM (FEI Tecnai G2 F30, Thermo Fisher Scientific, Waltham, MA, USA) at an accelerating voltage of 300 kV. Selected area electron diffractometry (SAED) was preformed using centered dark-field imaging.

2.6. X-ray diffractometry (XRD)

The crystal structure of mineralized collagen samples (1d-M and 2d-M) was determined using a Bruker D8 Advance diffractometer (40 kV, 40 mA) with Cu K_α radiation (Billerica, MA, USA) at a scanning rate of 0.02°/s and 2θ of 10°–75° range. Pristine collagen (0d-M) was analyzed by XRD as a control. To prepare XRD specimens, lyophilized samples were grounded into fine powders using a mortar and pestle and distributed in a groove silicon sample holder before testing.

2.7. Thermogravimetric analysis (TGA) and derivative thermogravimetry (DTG)

Thermal analysis of mineralized collagen samples was performed with TGA equipment with appropriate software (STARe System, Mettler Toledo, Columbus, OH, USA). Lyophilized mineralized and pristine collagen samples were placed in a 900 μL alumina pan. The temperature was raised from 30 °C to 800 °C at a constant heating rate of 10 °C/min in N_2. DTG was plotted as the first derivative of TGA data.

2.8. Rheology

Rheological properties were measured using a MCR 302 modular compact rheometer (Anton Paar, Graz, Austria) with a set of parallel plates of 8 mm in diameter. A cover was used to prevent water evaporation and to keep temperature constant at 25 °C. The samples were placed between plates with a 1 mm gap at the measuring position. Excess water was removed using Kimwipes® before each measurement. The measurement was performed using a frequency sweep with two intervals. In the first interval, the sample was equilibrated with a strain of 0.1% and an angular frequency of 0.1 rad/s for 5 min. In the second interval, the strain was maintained at 0.1% and the angular frequency was raised from 0.1 rad/s to 100 rad/s in a logarithmic ramp over 30 points. The time interval for each point was set from 10 s to 0.1 s in a logarithmic ramp. The measurements were recorded in triplicate for each group.

2.9. Loading and release of GL13K peptides from mineralized collagen gels

The amount of GL13K loaded and released from pristine and mineralized collagen was quantified by spectrofluorimetry [36]. Tetramethylrhodamine (TAMRA) fluorescently-tagged GL13K peptide (GKIIKLKASLKLLK-5-TAMRA; > 98% purity, AAPPTec, LLC, Louisville, KY, USA) was used for this purpose. TAMRA fluorophore has excitation and emission maxima at 550 nm and 578 nm, respectively. The fluorescence intensities for all the aqueous solutions were recorded using excitation and emission filters of 530 (±25) nm and 590 (±25) nm, respectively, using a multimode microplate reader (BioTek, Winooski, VT, USA). The calibration curve was constructed to obtain the linear relationship between peptide concentrations and relative fluorescence intensities. Firstly GL13K-TAMRA was dissolved in DI water at 1.4 mg/mL. The pristine and mineralized collagen gels were incubated in 250 μL of the GL13K-TAMRA solution for 15 min at room temperature. Subsequently, the supernatants and solutions from three consecutive washings of the samples were collected for measuring the remnant peptide concentrations. The difference in the concentrations of the GL13K-TAMRA before and after incubation with the collagen samples was used as a measure of the loaded peptide. For the release kinetics, the GL13K-TAMRA coated gels were incubated in 1 mL of Tris-buffered saline (TBS, pH = 7.6) and the buffer aliquots were assayed periodically to measure the cumulative peptide release. Each experiment was repeated twice.

Fluorescence microscopy was performed to visualize the distribution of GL13K-TAMRA on coated pristine and mineralized collagen samples. Micrographs were obtained with a confocal laser scanning microscope (CLSM; Olympus FluoView FV1000, Tokyo, Japan) at 10 × magnification. Micrograph analysis and visualization were performed in Fiji (available at https://fiji.sc/) adjusting for background from non-coated controls at each time point. Four fields of view from three samples per group were collected.

2.10. Water contact angle (WCA) measurement

Hydrophobicity of pristine and mineralized collagen, before and after coating with GL13K, was determined. Lyophilized collagen samples were flattened by pressuring them between two glass slides using a load of 0.5 lb. WCA on the flattened gels was determined with the sessile-drop method using a contact angle goniometer (DM-CE1, Kyowa Interface Science, Niiza-City, Japan). 2.0 μL of DI water was dispensed on the tested surface and contact angles of the water droplets with the tested surfaces were tracked over 60 s using the FAMAS software (Kyowa Interface Science, Niiza-City, Japan). Four samples were tested for each group.

2.11. Antimicrobial test

2.11.1. Bacterial culture

Gram-positive *Streptococcus gordonii* M5 and Gram-negative *Escherichia coli* DH5-α were used as bacterial models to test the antimicrobial activity of the hybrid GL13K coated and mineralized collagen samples. *S.gordonii* is a primary colonizer of oral surfaces that provides attachment for the subsequent pathogenic biofilm and dental plaque formation [37]. *E. coli* contains many pathotypes that can cause a variety of diseases [38] and is often used as a model pathogen for testing anti-infective preventive and therapeutic materials. *S.gordonii* was inoculated in Todd-Hewitt broth (THB; BD, Franklin Lakes, NJ, USA) and incubated for 24 h in a 5% CO_2 incubator at 37 °C and 100 rpm. *E. coli* was inoculated in brain heart infusion (BHI; BD, Franklin Lakes, NJ, USA) broth and incubated for 24 h in an aerobic incubator at 37 °C and 100 rpm. *S.gordonii* solution was diluted to 9.6×10^7 colony forming unit (CFU)/mL in THB and *E. coli* solution was diluted to 6.3×10^7 CFU/mL in BHI, respectively.

Pristine and mineralized collagen samples without GL13K were disinfected using ethanol before antimicrobial tests. The samples were immersed in 50% ethanol for 20 min at room temperature and then transferred into 70% ethanol overnight at 4 °C. After disinfection, the samples were transferred to 50% ethanol first and then washed with autoclaved DI water for three times. Ethanol was further removed by soaking the samples in autoclaved DI water overnight at 4 °C. After disinfection, GL13K-coated samples were prepared by soaking in a 1.0 mM GL13K solution of autoclaved DI water for 15 min followed by washing with autoclaved DI water for three times.

The disinfected samples were placed in 48-well plates with 0.5 mL/well of the diluted *S. gordonii* or *E. coli* solution and incubated for 24 h at 37 °C and 100 rpm, either in a 5% CO_2 incubator or an aerobic incubator, respectively.

2.11.2. ATP bioluminescence assay

Viability of microbial cells grown on the different collagen samples was quantified using the BacTiter-Glo™ Microbial Cell Viability Assay (Promega, Madison, WI, USA). After bacterial growth, the samples were washed by 1 × PBS twice and transferred to a new 48-well plate. An equal volume (200 μL) of BacTiter-Glo™ Reagent and 1 × PBS was added to each well. After incubating in dark at room temperature for 5 min, 200 μL of the mixture was transferred into a black 96-well plate and the emitted luminescence was detected using a multimode microplate reader (BioTek, Winooski, VT, USA). The control test group consisted of collagen samples immersed in culture medium without bacteria. Each experiment included four samples per group and was repeated in triplicate.

2.11.3. Live/dead assay

Live/Dead assay was performed to visualize microbial colonization and qualitatively compare bacterial viability between the different tested groups. Bacteria with intact membranes fluoresce green, whereas bacteria with compromised membranes fluoresce red. To prepare the staining solution, 3 μL of SYTO® 9 stain and 3 μL of propidium iodide stain from a LIVE/DEAD® Biofilm Viability Kit (Invitrogen, Carlsbad, CA, USA) were added to 1 mL of 1 × PBS. Each sample was incubated in 200 μL of the staining solution in dark at room temperature for 15 min and then washed with 1 × PBS and imaged immediately. To obtain a better description of the biofilm in the 3D hydrogel, we compressed the 3D gel to a flat thin membrane between the glass slide and cover slip so that multiple layers could be imaged at one plane. Micrographs were obtained by CLSM (Olympus FluoView FV1000, Tokyo, Japan) at 10 × for at least two fields per group in three independent experiments and processed in Fiji (available at https://fiji.sc/).

2.12. Cytotoxicity test

Pristine and mineralized collagen samples were disinfected using ethanol before cytotoxicity tests, as described above. Non-coated and GL13K-coated samples were immersed (1.5 cm^2 sample/ml media) in α-minimum essential medium (StemCell Technologies, Vancouver, Canada) supplemented with 1 × penicillin/streptomycin (Gibco, Thermo Fisher Scientific, Waltham, MA, USA), and 10% fetal bovine serum (Gibco, Thermo Fisher Scientific, Waltham, MA, USA). Extracts were collected at 2 weeks and 4 weeks and used for cytotoxicity assessment. Human bone marrow-derived mesenchymal stromal cells (hBM-MSCs) were kindly provided by the Tolar lab at the University of Minnesota. Cells were cultured in α-minimum essential medium supplemented with 1 × penicillin/streptomycin, 10% fetal bovine serum, and 1 ng/mL basic fibroblast growth factor (R&D Systems, Inc., Minneapolis, MN, USA) at 37 °C in a 5% CO_2 humidified incubator. Passage

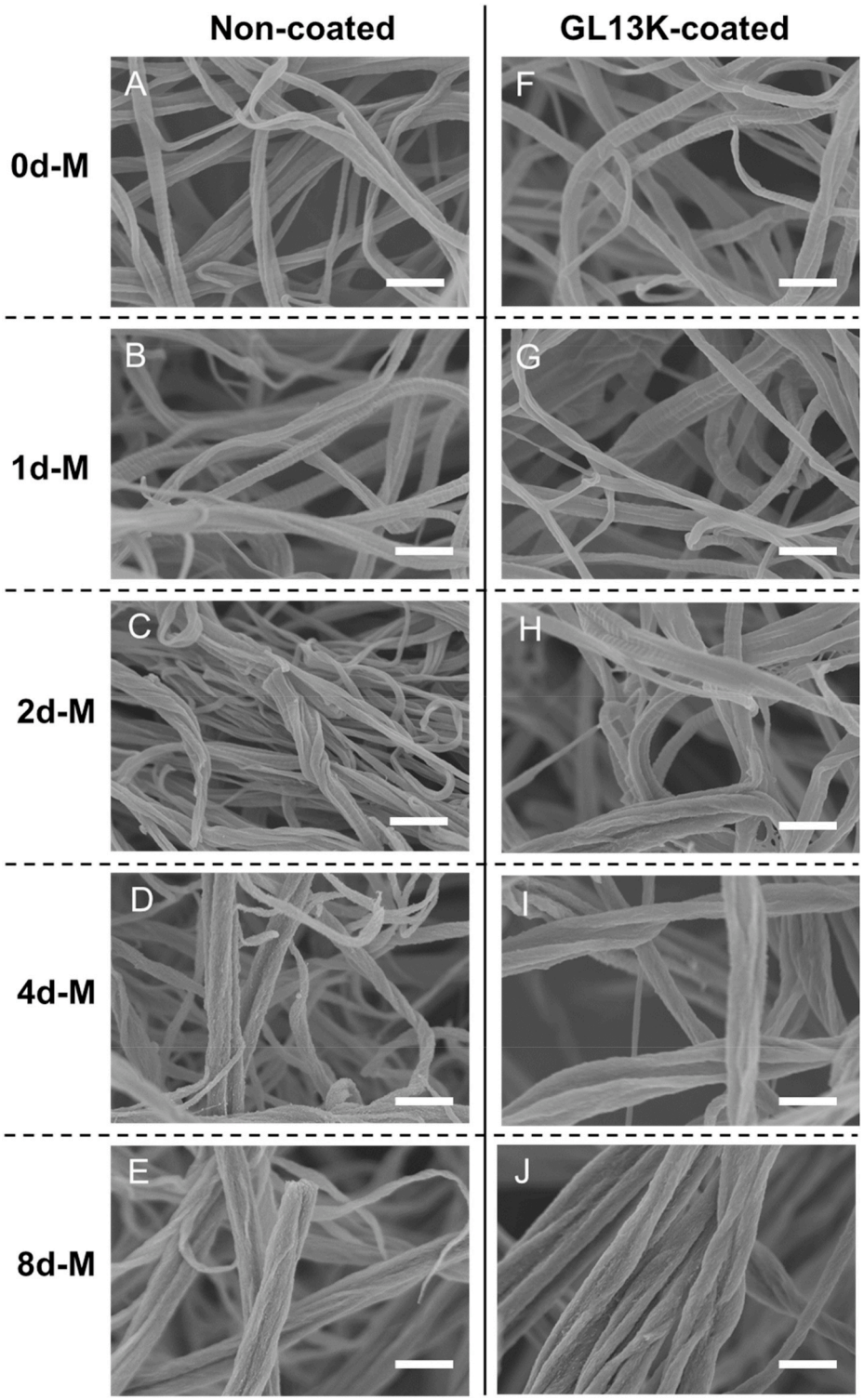

Fig. 1. Morphology of pristine and mineralized collagen fibrils. SEM micrographs of lyophilized collagen gels mineralized for 0 d, 1 d, 2 d, 4 d and 8 d without (A–E) and with (F–G) GL13K coating. The GL13K coating did not modify the morphology of collagen fibrils. Scale bars are all 500 nm.

4 cells were used for cytotoxicity assessment of collected extracts. Cells were passaged and plated in a 48-well plate at a density of 10,000 cells/cm^2 in 500 μl media and cultured for 24 h. After 24 h, media was replaced with 500 μl of extract or fresh serum supplemented media (negative control) or different concentrations of ethanol (4%, 5% and 7.5%) as positive controls. Cells were incubated for additional 48 h and then characterized using CCK8 assay (Dojindo, Rockville, MD, USA) to determine extract-mediated cytotoxicity. CCK8 assay was performed following manufacturer's instruction. Briefly, after 48 h incubation, extract was replaced with fresh media containing 10% CCK8 reagent and cells were incubated for additional 2 h. The reduction of the CCK8 reagent was quantified colorimetrically by measuring absorbance at 450 nm using a multimode microplate reader (BioTek, Winooski, VT, USA). The absorbance measured was normalized against negative controls to determine extract dependent toxicity. Three samples were used for each group.

2.13. Statistical analysis

Statistical analysis was performed using IBM SPSS Statistics Version 25. Normality was assessed by the Kolmogorov-Smirnov test and homogeneity of variances was assessed by the Levene's test. The luminescence intensity for *S. gordonii* had non-homogeneous variances and was compared by one-way ANOVA with Dunnett T3 post hoc test. The luminescence intensity for *E. coli*, the cell viability percentage, and the physical and chemical properties of the collagen gels had homogeneous variances and were compared by one-way ANOVA with Tukey post hoc test. The statistical significance level was set at 0.05.

3. Results

3.1. Biomimetic mineralization of collagen gels for different days

The collagen scaffolds were composed of a network of reconstituted collagen fibrils with diameters of around 50–200 nm and characteristic periodic banding patterns (Fig. 1A). After mineralization for one day (1d-M), the collagen fibrils did not have notable morphological changes compared to 0d-M and preserved the periodic banding (Fig. 1B). However, HA was present in the 1d-M samples as XRD spectra showed HA characteristic peaks for the (002) and overlapping (211), (112) and (300) families of planes (Fig. 2A). After 2 days of mineralization further growth of HA crystals inside the collagen fibers partially masked the periodic banding (2d-M, Fig. 1C) and increased the intensity of the characteristic XRD peaks for HA: (002), (210), (310), (222) and (213) (Fig. 2A). Notably, all samples were cut in half after lyophilization to reveal the center of the mineralized collagen scaffolds, which were the zones visualized by SEM and shown in Fig. 1. Thus, Fig. 1D and E demonstrated that 4d-M and 8d-M samples were intrafibrillarly mineralized in full with a homogenous and high degree of mineralization across the scaffold. Higher magnification SEM and bright-field TEM analysis of the fully mineralized collagen fibrils further confirmed the complete infiltration of HA nanocrystals inside the collagen fibrils (Fig. 2B and C). The arcing of the (002) planes in the SAED pattern indicated that the *c*-axis of the HA nanocrystals were aligned along the [001] direction, which was also parallel to the long axis of the analyzed collagen fibril. This ultrastructural bone biomimetic feature of the obtained mineralized fibers is characteristic of mineralized reconstituted collagen fibrils using PILP processes [15].

We used TGA to quantify the mineral content in mineralized samples after different mineralization periods. The residual weight percentage at 800 °C increased in the mineralized gels with increased mineralization time, which indicated that the gels continued to incorporate intrafibrillar minerals over the whole period of the PILP process (Fig. 3A). The small 5% residual mineral increase from day 4 to day 8 of mineralization suggested that the collagen scaffolds were near complete intrafibrillar mineralization after 4 days in the mineralization solution. DTG analysis showed a low temperature peak raging 30–100 °C that corresponded to the loss of physisorbed water and a high temperature peak in the broad range 200–500 °C that corresponded to the decomposition (250–350 °C) of the collagen matrix (Fig. 3B). The collagen decomposition peak progressively shifted to higher temperatures as the time of mineralization increased, which suggests the intimate structural connectivity between collagen and HA as the crystals were embedded within the collagen fibrils [16]. This has been previously shown for collagen in natural mineralized tissues [39].

We conducted rheological analysis of pristine and mineralized collagen samples. All groups showed a distinguishable gel-like behavior [40]. The storage modulus (G′) was higher than the loss modulus (G″) across all frequencies measured for all tested samples (Fig. 3C and D). Both G′ and G″ increased with the increasing degree of mineralization, indicating that the presence of HA enhanced the stiffness of the collagen matrix and also imparted a paste-like viscous nature to the mineralized gel [41]. The small increase of mineral content between 4d-M and 8d-M (5 wt%, Fig. 3A) induced a notable one-magnitude increase of both G′ and G". This significant increase in moduli suggests that even after the collagen fibrils were almost fully infiltrated with HA (4d-M, Fig. 1D), further mineralization completed the process of intrafibrillar mineral infiltration, which significantly stiffened the collagen gels.

3.2. Loading and release of GL13K antimicrobial peptides

TAMRA fluorescently-tagged GL13K (GL13K-TAMRA) was coated on pristine and mineralized collagen gels to study the loading and release of GL13K. A standard plot of GL13K-TAMRA concentration versus emission

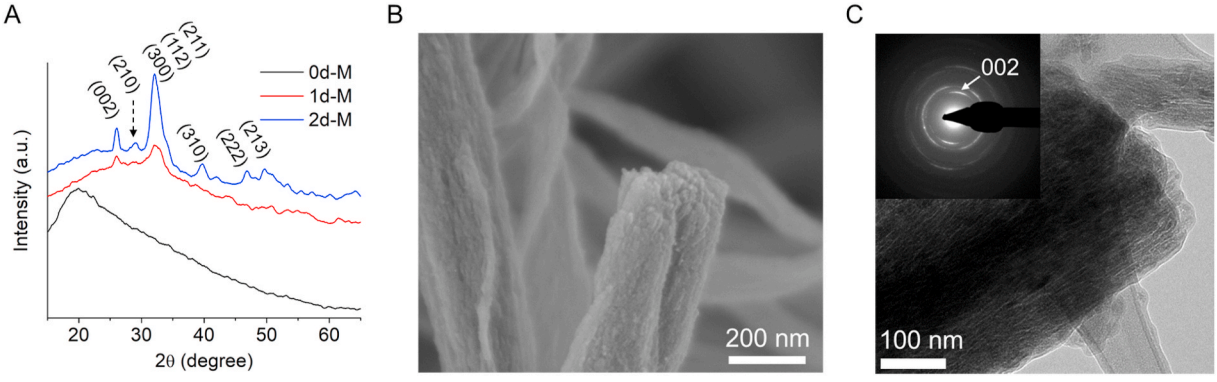

Fig. 2. Structural characterization of intrafibrillarly mineralized collagen. (A) XRD spectra of collagen gels before mineralization (0d-M) and after being mineralized for 1 d and 2 d. Characteristic peaks for HA are labeled. (B) High-magnification SEM micrograph of 8d-M collagen showing thorough infiltration of HA minerals in the collagen fibrils. (C) TEM micrograph of 8d-M collagen. Insert is the SAED pattern of the imaged collagen fibril.

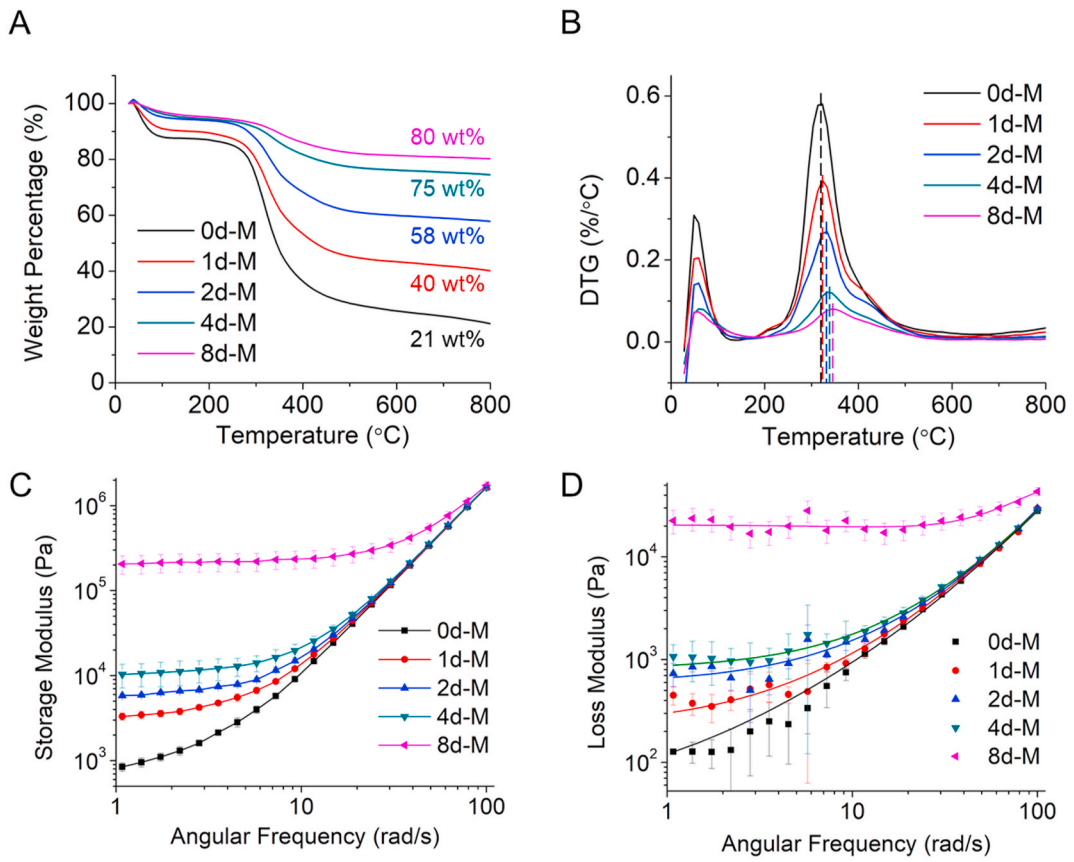

Fig. 3. Thermal decomposition and rheological analysis of pristine and mineralized collagen. (A) TGA and (B) DTG analysis of collagen samples before and after mineralization for different periods. Dash lines in (B) highlight the shift of the temperature for collagen decomposition. (C) Storage and (B) loss moduli of non-mineralized and mineralized collagen gels as a function of angular frequency.

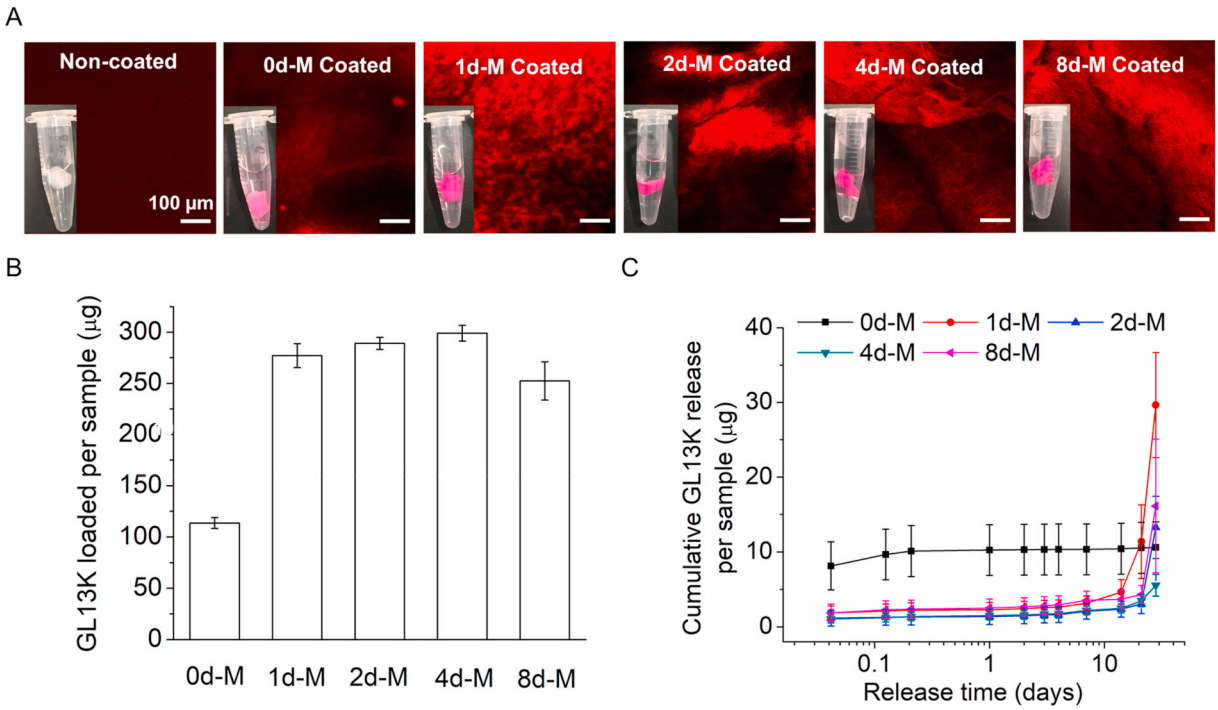

Fig. 4. GL13K-TAMRA peptide loading and release from peptide-coated collagen scaffolds. (A) CLSM micrographs of pristine non-mineralized and mineralized collagen samples with and without GL13K-TAMRA coating. All scale bars are 100 μm. Inserts are digital photographs of the hydrogels in waters. (B) Quantification of GL13K-TAMRA loaded on non-mineralized and mineralized collagen scaffolds. (C) Cumulative GL13K-TAMRA release for up to 28 days from non-mineralized and mineralized collagen scaffolds.

fluorescence intensity with a linear slope and y-axis intercept was used to measure the peptide concentrations in the aqueous solutions. The digital macrographs and CLSM micrographs shown in Fig. 4A indicated a higher affinity and thus, loading of GL13K-TAMRA to the mineralized fibrillar collagen scaffolds (1d-M, 2d-M, 4d-M and 8d-M) than to the non-mineralized pristine collagen scaffolds (0d-M). Quantification of the peptide loaded per sample (Fig. 4B) confirmed the higher affinity of GL13K-TAMRA to the mineralized gels compared to the pristine collagen. However, no significant differences were assessed for GL13K-TAMRA loaded in mineralized collagens after different periods of mineralization (1, 2, 4 and 8 days). Cumulative GL13K-TAMRA release (Fig. 4C) from the mineralized collagen scaffolds was nearly negligible up to 14 days in solution followed by burst release from 21 to 28 days probably due to the hydrolysis of collagen. This was in contrast to the almost immediate and full release of the peptide from the non-mineralized collagen (0d-M).

The loading of the scaffolds with GL13K did not change the morphology of the collagen fibrils in any collagen scaffolds (Fig. 1F–J), but significantly changed hydrophobicity of the mineralized collagen scaffolds (Fig. 5). Mineralization of the collagen scaffolds as well as GL13K coatings induced significant changes in scaffold wettability. Non-mineralized pristine collagen was highly hydrophobic whereas all scaffolds were highly hydrophilic after mineralization (Fig. 5A and C). GL13K peptides changed the wettability of mineralized collagen scaffolds. All GL13K-coated substrates were highly hydrophobic with minimal dynamic response (Fig. 5B and D), which indicated the stability of the peptide molecules while interacting with water.

3.3. Antimicrobial activity of GL13K coated mineralized collagen

The antimicrobial activity of GL13K coating was assessed against Gram-positive *S. gordonii* and Gram-negative *E. coli*. The viability of the bacteria after being exposed for 24 h in contact with the peptide-coated collagen samples was quantified with the ATP assay (Fig. 6). GL13K coatings significantly reduced the viability of *E. coli* in all non-mineralized and mineralized collagen scaffolds (Fig. 6B). However, a statistically significant reduction in *S. gordonii* viability for GL13K-coated collagen scaffolds was only observed in scaffolds mineralized for 2 days or longer; i.e., with notable degree of mineralization. The mineral presence itself had an impact on *S. gordonii* colonization as well. There was a significant increase of *S. gordonii* viable cells as the content of HA in the scaffolds increased for groups either without or with GL13K coatings. The same correlation was found for the number of viable *E. coli* in non-coated scaffolds, but it was less significant than in the case of *S. gordonii*. The direct relation between amount of mineral and viable bacteria might indicate a preference of these two strains to attach to increasingly rigid scaffolds. Others have shown similar correlations between *Staphylococcus aureus* and *E. coli* and non-mineralized polymeric hydrogels with different rigidity [42].

The reduced viable bacteria numbers on the GL13K coated collagen gels correlated with the number of bacteria with compromised membranes as shown in the Live/Dead fluorescence images (Fig. 7). More red *S. gordonii* were imaged on the samples with GL13K coating compared to that without coating, except for 0d-M and 1d-M scaffolds. GL13K coatings had more notable effects on the membrane integrity of *E. coli* than *S. gordonii*, suggesting that *E. coli* are more susceptible to GL13K activity than *S. gordonii*.

3.4. Cytocompatibility

The cytotoxicity of the collagen scaffolds without or with GL13K coating was assessed against hBM-MSCs, a relevant cell type for bone regeneration. None of the scaffolds tested showed cytotoxic effects. The metabolic viability of hBM-MSCs grown with extracts of media exposed

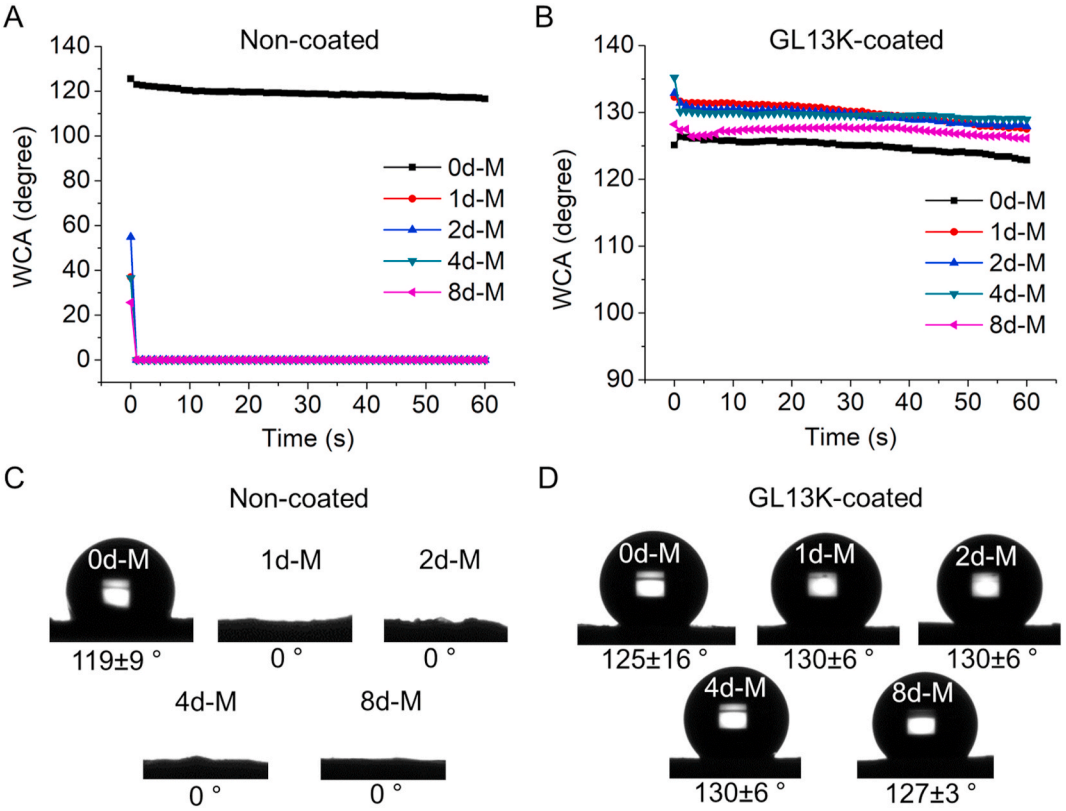

Fig. 5. Wettability of collagen with/without mineralization and with/without GL13K peptide coatings. (A, B) Dynamic WCA on non-mineralized and mineralized collagen without and with GL13K coating. (C, D) Representative photographs of water droplets on tested specimens and averaged WCA ± standard deviation at t = 60 s for each group of tested samples.

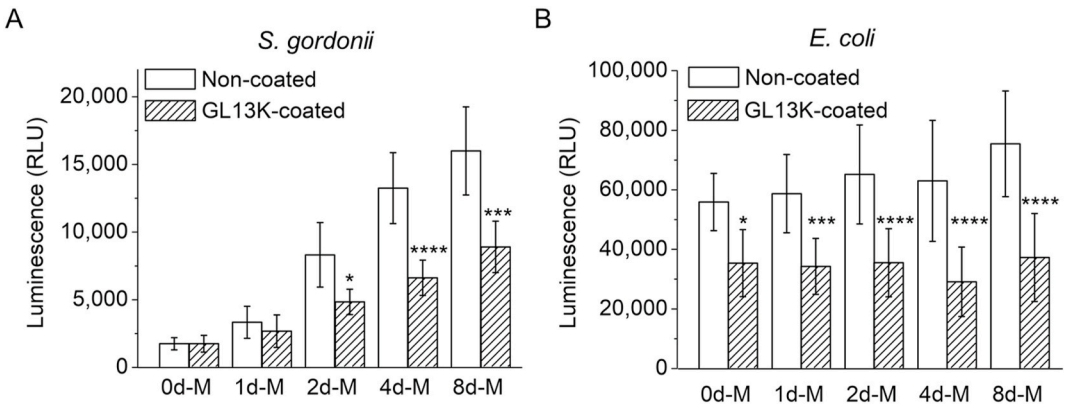

Fig. 6. Bacteria viability on collagen scaffolds with/without mineralization and with/without GL13K peptide coatings. ATP luminescence of (A) *S. gordonii* and (B) *E. coli* cultured with non-mineralized and mineralized collagen gels without and with GL13K coating. Statistical significance (* p-value<0.05, ***p-value<0.001, ****p-value<0.0001, n = 12) indicates differences between non-coated and GL13K-coated samples at each mineralization period.

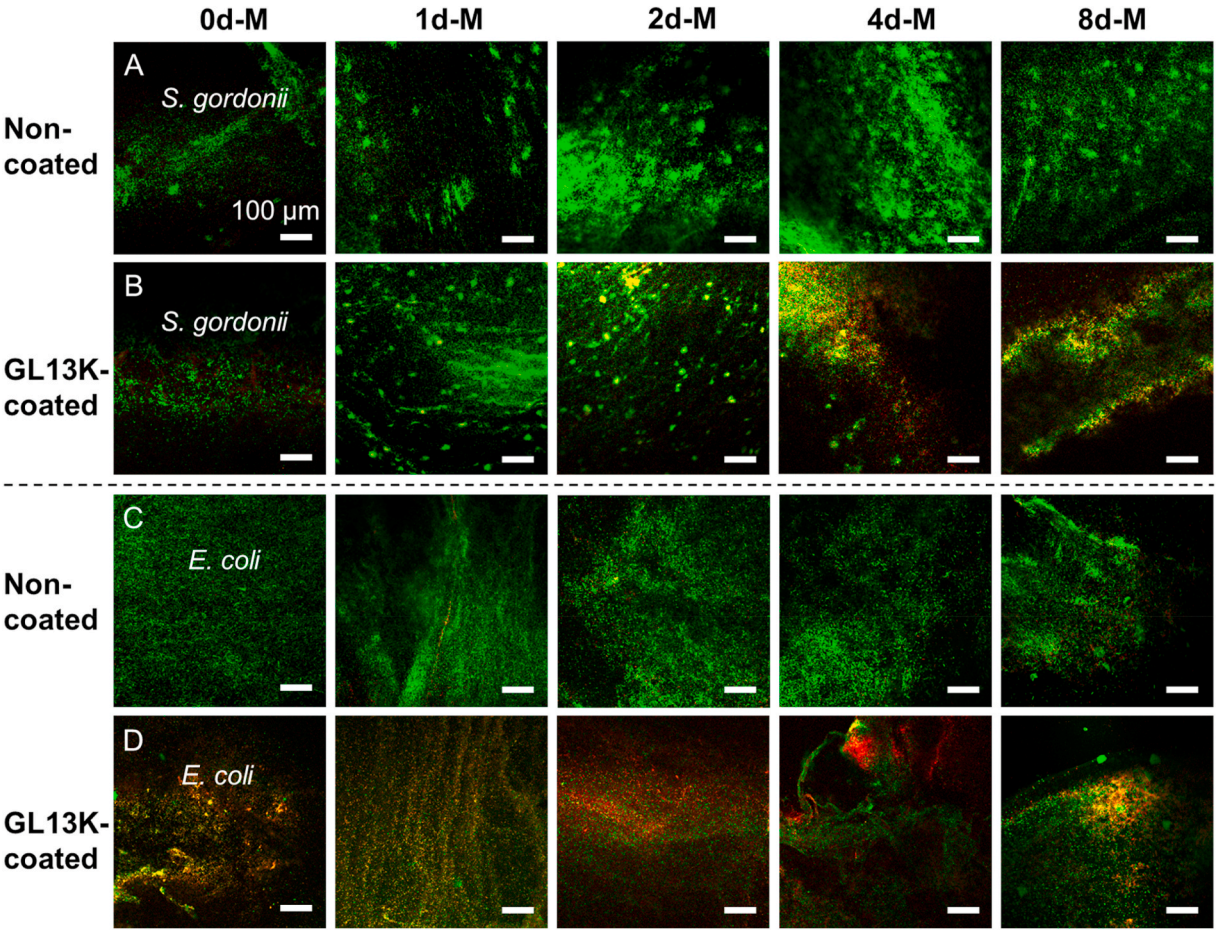

Fig. 7. Visualization of bacteria with intact (green) or compromised (red) cell membrane on collagen scaffolds. LIVE/DEAD CLSM micrographs of (A, B) *S. gordonii* and (C, D) *E. coli* cultured on non-mineralized (0d-M column) and mineralized (1d-M, 2d-M, 4d-M, 8d-M columns) collagen scaffolds without (A, C) and with (B, D) GL13K coating. Scale bars are all 100 μm.

to each of the different scaffolds was not significantly different than that of the cells grown with serum supplemented media; i.e., with the negative control (Fig. 8). A significant reduction in cell metabolic activity was assessed in cell grown in media with increasing ethanol concentration; i.e., with positive controls. These results suggested that none of the degraded/eluted products from collagen, minerals and adsorbed GL13K were cytotoxic or released in sufficient concentration to be cytotoxic to hBM-MSCs [43].

4. Discussion

As infection is a relevant associated risk in bone and dental regeneration therapies, here we validated the antimicrobial effects of the GL13K peptides absorbed in the mineralized collagen scaffolds against two model bacteria, *S. gordonii* and *E. coli*. Previous works have shown the broad-spectrum activity of GL13K against other pathogenic bacteria, such as *Pseudomonas aeruginosa*, *Porphyromonas gingivalis*, *Fusobacterium*

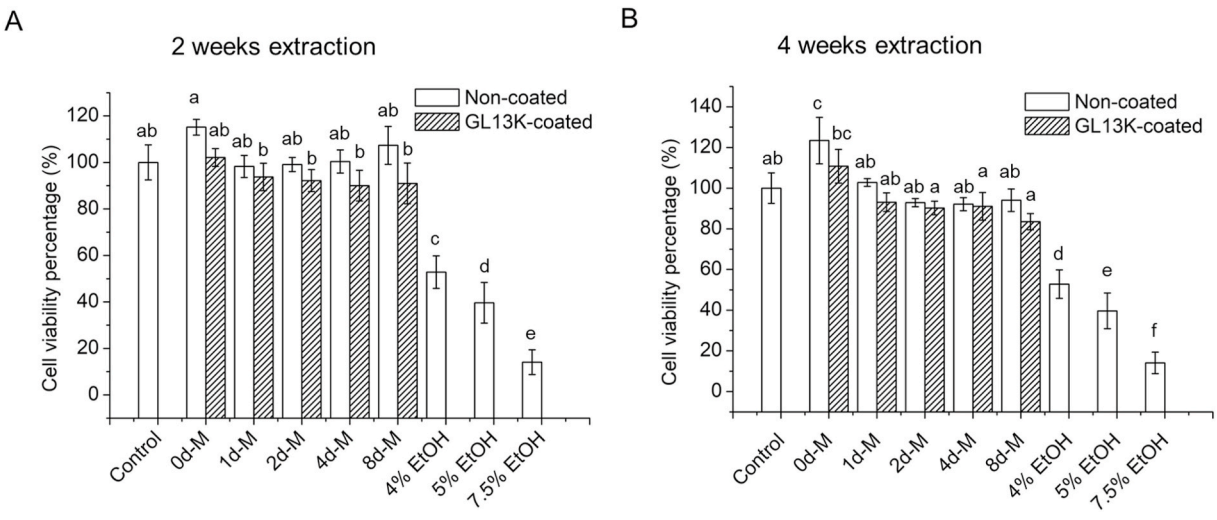

Fig. 8. Cytotoxicity of eluents from collagen scaffolds. hBM-MSCs metabolic viability (CCK8) percentages with respect to control group exposed to extracts with eluents released from non-mineralized (0d-M) and mineralized collagen scaffolds without and with GL13K coatings after (A) 2 weeks and (B) 4 weeks of incubation in cell culture medium. Control: cell culture medium negative control. 4%, 5% and 7.5% EtOH: culture medium with 4%, 5%, and 7.5% ethanol positive controls. Different letters indicate statistically significant differences between groups (p-value<0.05).

nucleatum, *Enterococcus faecalis*, *Staphylococcus aureus* and methicillin-resistant *S. aureus* both *in vitro* [35,44] and *in vivo* [45] as well as in solution [46] and as coatings on different substrates [47,48]. The antimicrobial potency of the GL13K coating was more noticeable against the Gram-negative *E. coli* than the Gram-positive *S. gordonii* bacteria. Previous work showed similar effects as GL13K had lower MICs against Gram-negatives than Gram-positives [33,49]. This has been tentatively attributed to different modes of action of the cationic AMPs as the peptides can differently interact with the outer membrane of Gram-negative bacteria or the cell wall of Gram-positive bacteria [50]. Our results support that the antimicrobial activity of the GL13K coatings was mostly by contact killing as release of GL13K from the scaffold was negligible for up to 14 days. We have previously shown that GL13K peptide coatings are potent and stable when formed on dentin with undetectable release of the AMPs when exposed to simulated saliva [9]. We also showed that the peptide preferably adsorbed on highly mineralized regions of the dentin structure, which is in agreement with the higher amount of peptide incorporated in our mineralized collagen scaffolds. The strong binding of GL13K provides a durable antimicrobial potency to the scaffolds that can protect against infection for sustained periods during bone regeneration, which can take from weeks to months [51]. The high stability of the GL13K coatings has been related to the ability of the peptides to self-assemble [49,52]. Moreover, recruitment of the AMPs to form the coatings was favored when the peptides interacted with highly polar, highly hydrophilic substrates [53]. This was attributed to the amphipathic nature of GL13K and their supramolecular structures. Thus, the highly hydrophilic mineralized collagen scaffolds provided an ideal substrate to form coatings with large loading of AMPs.

The coating of amphipathic GL13K peptides with the orientation of the hydrophobic residues facing towards the solid-air interface remarkably increased hydrophobicity of the scaffold, which may retard degradation of the coating by protecting it from hydrolysis and other water-borne agents including enzymes [54]. Without GL13K coating, the minerals added to the scaffold increased the amount of bacterial attachment, which was more significant for *S. gordonii* than for *E. coli*. The minerals routinely incorporated in hard tissue engineering scaffolds can be a sort of a double-edged sword as on the one side, the minerals promote bone/dental tissue regeneration; but on the other side, the minerals favor attachment of bacteria due to their highly hydrophilic nature [55]. To that end, it is of relevance that these scaffolds incorporate antimicrobial agents, like our GL13K peptides here, so that they can provide protection against infections after implantation.

The GL13K-coated mineralized scaffolds were not cytotoxic, which we attributed to the stability of the AMPs coatings as per our previous discussion. The cytocompatibility of the GL13K coatings with other mammalian cells (osteoblasts [35], fibroblasts [9], and keratinocytes [47]) has also been demonstrated when the cells were in direct contact with the AMP coating. Future comprehensive studies with our GL13K-coated mineralized collagen scaffolds will focus on assessing their *in vitro* osteogenic properties so that we can assess not only the effectiveness of the minerals, but also the effects of the AMP coatings, both from a biological and physicochemical (hydrophobicity) standpoint, to induce osteoblastic differentiation. Our previous work showed that the hydrophobicity of the GL13K coatings on titanium did not significantly affect *in vivo* osseointegration [56].

The use of the PILP process for intrafibrillar mineralization of our hybrid scaffolds provides an array of options for tuning properties and developing further the scaffolds. For instance, using the PILP process enabled here modification of the percentage of inorganics and so, the rheological behavior of the scaffolds. We controlled the weight percentage of minerals, which ranged from around 20%–60%, by controlling the time duration of mineralization of the scaffolds. As the increased amount of mineral did not affect the scaffold hydrophilicity or increased the nanofiber surface area, the amount of GL13K in the coatings reached saturation for scaffolds with the minimum mineral content (1d-M). Thus, further mineralizing the collagen did not affect the amount of GL13K coatings, but increased the scaffold's mechanical properties. Generating a gradient scaffold using this system would be feasible by immersing different parts of the scaffold in the PILP mineralization solution for different periods. This would be useful to fabricate biomimetic scaffolds applied in soft-to-hard tissue interfaces, such as tendon enthuses, ligament insertions, osteochondral zones, and periodontium [57]. Moreover, the versatility of the PILP process can be further exploited as it can be used to mineralize scaffolds with alternative nanofibrillar polymers, such as cellulose and elastin like polymers [58,59] or collagen fibers with calcium phosphates modified with ions, such as magnesium and strontium [60–62], with known osteogenic potential.

5. Conclusions

We developed a hybrid scaffold based on intrafibrillarly mineralized collagen that was coated with the designer antimicrobial peptide, GL13K. Our scaffold had nanostructural features similar to those in tissues with mineralized collagen matrices, was not cytotoxic and had

antimicrobial potency against Gram-positive and Gram-negative bacteria.

CRediT authorship contribution statement

Zhou Ye: Conceptualization, Funding acquisition, Methodology, Formal analysis, Writing - original draft. **Xiao Zhu:** Methodology, Formal analysis. **Isha Mutreja:** Methodology, Formal analysis. **Sunil Kumar Boda:** Methodology, Formal analysis, Writing - review & editing. **Nicholas G. Fischer:** Methodology, Formal analysis, Writing - review & editing. **Anqi Zhang:** Methodology, Formal analysis. **Christine Lui:** Methodology. **Yipin Qi:** Conceptualization. **Conrado Aparicio:** Conceptualization, Resources, Funding acquisition, Supervision, Writing - review & editing.

Declaration of competing interest

The authors declare no conflicts of interest.

Acknowledgements

The authors acknowledge Professor Sven Gorr, Ms. Ruoqiang Chen, and Professor Jakub Tolar from the University of Minnesota for donating *S. gordonii, E. coli,* and hBM-MSCs, respectively. The authors also acknowledge Neus Bahí Vives from Eurecat for technical assistance with the TGA/DTG analysis. This research was supported by the National Institute for Dental and Craniofacial Research of the National Institutes of Health [grant number R01DE026117 to C. A., T90DE0227232 to N.G. F.], the National Institutes of Health's National Center for Advancing Translational Sciences [Translational Research Development Program-TRDP award to Z.Y. from grant UL1TR002494], the Fundamental Research Funds for the Central Universities [grant number 2042020kf0191 to X.Z.], the National Natural Science Foundation of China [grant number 81400506 to Y.Q.] and the Natural Science Foundation of Guangdong Province [grant number 2018B030311040 to Y.Q.]. NGF acknowledges support from a 3 M Science and Technology Fellowship. The content is solely the responsibility of the authors and does not necessarily represent the official views of the National Institutes of Health. Parts of this work were carried out in the University of Minnesota I.T. Characterization Facility, which receives partial support from NSF through the MRSEC program. Confocal laser scanning microscopy was performed at the University of Minnesota – University Imaging Center.

References

[1] K. Okike, T. Bhattacharyya, Trends in the management of open fractures: a critical analysis, J. Bone Jt. Surg. - Ser. A. 88 (2006) 2739–2748, https://doi.org/10.2106/JBJS.F.00146.

[2] M.B. Nair, J.D. Kretlow, A.G. Mikos, F.K. Kasper, Infection and tissue engineering in segmental bone defects-a mini review, Curr. Opin. Biotechnol. 22 (2011) 721–725, https://doi.org/10.1016/j.copbio.2011.02.005.

[3] P.A. Norowski, J.D. Bumgardner, Biomaterial and antibiotic strategies for peri-implantitis, J. Biomed. Mater. Res. B Appl. Biomater. 88 (2009) 530–543, https://doi.org/10.1002/jbm.b.31152.

[4] D.G. Moussa, C. Aparicio, Present and future of tissue engineering scaffolds for dentin-pulp complex regeneration, J. Tissue Eng. Regen. Med. 13 (2019) 58–75, https://doi.org/10.1002/term.2769.

[5] A. Al-Ahmad, M. Wiedmann-Al-Ahmad, C. Carvalho, M. Lang, M. Follo, G. Braun, A. Wittmer, R. Mülhaupt, E. Hellwig, Bacterial and Candida albicans adhesion on rapid prototyping-produced 3D-scaffolds manufactured as bone replacement materials, J. Biomed. Mater. Res. - Part A. 87 (2008) 933–943, https://doi.org/10.1002/jbm.a.31832.

[6] Y. Yang, L. Chu, S. Yang, H. Zhang, L. Qin, O. Guillaume, D. Eglin, R.G. Richards, T. Tang, Dual-functional 3D-printed composite scaffold for inhibiting bacterial infection and promoting bone regeneration in infected bone defect models, Acta Biomater. 79 (2018) 265–275, https://doi.org/10.1016/j.actbio.2018.08.015.

[7] M. Vallet-Regí, D. Lozano, B. González, I. Izquierdo-Barba, Biomaterials against bone infection, Adv. Healthc. Mater. 9 (2020), https://doi.org/10.1002/adhm.202000310, 2000310.

[8] D.G. Moussa, A. Fok, C. Aparicio, Hydrophobic and antimicrobial dentin: a peptide-based 2-tier protective system for dental resin composite restorations, Acta Biomater. 88 (2019) 251–265, https://doi.org/10.1016/j.actbio.2019.02.007.

[9] D.G. Moussa, J.A. Kirihara, Z. Ye, N.G. Fischer, J. Khot, B.A. Witthuhn, C. Aparicio, Dentin priming with amphipathic antimicrobial peptides, J. Dent. Res. 98 (2019) 1112–1121, https://doi.org/10.1177/0022034519863772.

[10] A.A. Al-Munajjed, N.A. Plunkett, J.P. Gleeson, T. Weber, C. Jungreuthmayer, T. Levingstone, J. Hammer, F.J. O'Brien, Development of a biomimetic collagen-hydroxyapatite scaffold for bone tissue engineering using a SBF immersion technique, J. Biomed. Mater. Res. B Appl. Biomater. 90 B (2009) 584–591, https://doi.org/10.1002/jbm.b.31320.

[11] M.M. Villa, L. Wang, J. Huang, D.W. Rowe, M. Wei, Bone tissue engineering with a collagen-hydroxyapatite scaffold and culture expanded bone marrow stromal cells, J. Biomed. Mater. Res. B Appl. Biomater. 103 (2015) 243–253, https://doi.org/10.1002/jbm.b.33225.

[12] J. Venugopal, S. Low, A.T. Choon, T.S. Sampath Kumar, S. Ramakrishna, Mineralization of osteoblasts with electrospun collagen/hydroxyapatite nanofibers, J. Mater. Sci. Mater. Med. 19 (2008) 2039–2046, https://doi.org/10.1007/s10856-007-3289-x.

[13] K.F. Lin, S. He, Y. Song, C.M. Wang, Y. Gao, J.Q. Li, P. Tang, Z. Wang, L. Bi, G. X. Pei, Low-temperature additive manufacturing of biomimic three-dimensional hydroxyapatite/collagen scaffolds for bone regeneration, ACS Appl. Mater. Interfaces 8 (2016) 6905–6916, https://doi.org/10.1021/acsami.6b00815.

[14] S. Weiner, H.D. Wagner, The material bone: structure-mechanical function relations, Annu. Rev. Mater. Sci. 28 (1998) 271–298, https://doi.org/10.1146/annurev.matsci.28.1.271.

[15] M.J. Olszta, X. Cheng, S.S. Jee, R. Kumar, Y.Y. Kim, M.J. Kaufman, E.P. Douglas, L. B. Gower, Bone structure and formation: a new perspective, Mater. Sci. Eng. R Rep. 58 (2007) 77–116, https://doi.org/10.1016/j.mser.2007.05.001.

[16] Y. Li, T.T. Thula, S. Jee, S.L. Perkins, C. Aparicio, E.P. Douglas, L.B. Gower, Biomimetic mineralization of woven bone-like nanocomposites: role of collagen cross-links, Biomacromolecules 13 (2012) 49–59, https://doi.org/10.1021/bm201070g.

[17] Y. Li, C. Aparicio, Discerning the subfibrillar structure of mineralized collagen fibrils: a model for the ultrastructure of bone, PloS One 8 (2013), https://doi.org/10.1371/journal.pone.0076782 e76782.

[18] L.N. Niu, S.E. Jee, K. Jiao, L. Tonggu, M. Li, L. Wang, Y.D. Yang, J.H. Bian, L. Breschi, S.S. Jang, J.H. Chen, D.H. Pashley, F.R. Tay, Collagen intrafibrillar mineralization as a result of the balance between osmotic equilibrium and electroneutrality, Nat. Mater. 16 (2017) 370–378, https://doi.org/10.1038/nmat4789.

[19] G. Thrivikraman, A. Athirasala, R. Gordon, L. Zhang, R. Bergan, D.R. Keene, J. M. Jones, H. Xie, Z. Chen, J. Tao, B. Wingender, L. Gower, J.L. Ferracane, L. E. Bertassoni, Rapid fabrication of vascularized and innervated cell-laden bone models with biomimetic intrafibrillar collagen mineralization, Nat. Commun. 10 (2019) 1–14, https://doi.org/10.1038/s41467-019-11455-8.

[20] Y. Wang, N. Van Manh, H. Wang, X. Zhong, X. Zhang, C. Li, Synergistic intrafibrillar/extrafibrillar mineralization of collagen scaffolds based on a biomimetic strategy to promote the regeneration of bone defects, Int. J. Nanomed. 11 (2016) 2053–2067, https://doi.org/10.2147/IJN.S102844.

[21] Y. Qi, Z. Ye, A. Fok, B.N. Holmes, M. Espanol, M.P. Ginebra, C. Aparicio, Effects of molecular weight and concentration of poly(acrylic acid) on biomimetic mineralization of collagen, ACS Biomater. Sci. Eng. 4 (2018) 2755–2766, https://doi.org/10.1021/acsbiomaterials.8b00512.

[22] J. Wang, Y. Qu, C. Chen, J. Sun, H. Pan, C. Shao, R. Tang, X. Gu, Fabrication of collagen membranes with different intrafibrillar mineralization degree as a potential use for GBR, Mater. Sci. Eng. C 104 (2019), https://doi.org/10.1016/j.msec.2019.109959, 109959.

[23] L. Yu, D.W. Rowe, I.P. Perera, J. Zhang, S.L. Suib, X. Xin, M. Wei, Intrafibrillar mineralized collagen-hydroxyapatite-based scaffolds for bone regeneration, ACS Appl. Mater. Interfaces 12 (2020) 18235–18249, https://doi.org/10.1021/acsami.0c00275.

[24] H. Nurrohman, K. Saeki, K.M.M. Carneiro, Y.C. Chien, S. Djomehri, S.P. Ho, C. Qin, L.B. Gower, S.J. Marshall, G.W. Marshall, S. Habelitz, Repair of dentin defects from DSPP knockout mice by PILP mineralization, J. Mater. Res. 31 (2016) 321–327, https://doi.org/10.1557/jmr.2015.406.

[25] Y. xuan Ma, S.E. Hoff, X. qing Huang, J. Liu, Q. qian Wan, Q. Song, J. ting Gu, H. Heinz, F.R. Tay, L. na Niu, Involvement of prenucleation clusters in calcium phosphate mineralization of collagen, Acta Biomater. (2020), https://doi.org/10.1016/j.actbio.2020.07.038.

[26] S.S. Jee, T.T. Thula, L.B. Gower, Development of bone-like composites via the polymer-induced liquid-precursor (PILP) process. Part 1: influence of polymer molecular weight, Acta Biomater. 6 (2010) 3676–3686, https://doi.org/10.1016/j.actbio.2010.03.036.

[27] N. Mookherjee, M.A. Anderson, H.P. Haagsman, D.J. Davidson, Antimicrobial host defence peptides: functions and clinical potential, Nat. Rev. Drug Discov. 19 (2020) 311–332, https://doi.org/10.1038/s41573-019-0058-8.

[28] G. Yang, T. Huang, Y. Wang, H. Wang, Y. Li, K. Yu, L. Dong, Sustained release of antimicrobial peptide from self-assembling hydrogel enhanced osteogenesis, J. Biomater. Sci. Polym 29 (2018) 1812–1824, https://doi.org/10.1080/09205063.2018.1504191.

[29] Y. He, Y. Jin, X. Ying, Q. Wu, S. Yao, Y. Li, H. Liu, G. Ma, X. Wang, Development of an antimicrobial peptide-loaded mineralized collagen bone scaffold for infective bone defect repair, Regen. Biomater. (2020), https://doi.org/10.1093/rb/rbaa015.

[30] M. Kazemzadeh-Narbat, J. Kindrachuk, K. Duan, H. Jenssen, R.E.W. Hancock, R. Wang, Antimicrobial peptides on calcium phosphate-coated titanium for the

prevention of implant-associated infections, Biomaterials 31 (2010) 9519–9526, https://doi.org/10.1016/j.biomaterials.2010.08.035.
[31] H. Yazici, G. Habib, K. Boone, M. Urgen, F.S. Utku, C. Tamerler, Self-assembling antimicrobial peptides on nanotubular titanium surfaces coated with calcium phosphate for local therapy, Mater. Sci. Eng. C 94 (2019) 333–343, https://doi.org/10.1016/j.msec.2018.09.030.
[32] C.H. Chen, T.K. Lu, Development and challenges of antimicrobial peptides for therapeutic applications, Antibiotics, https://doi.org/10.3390/antibiotics9010024, 2020.
[33] H. Hirt, S.U. Gorr, Antimicrobial peptide GL13K is effective in reducing biofilms of Pseudomonas aeruginosa, Antimicrob, Agents Chemother 57 (2013) 4903–4910, https://doi.org/10.1128/AAC.00311-13.
[34] X. Chen, H. Hirt, Y. Li, S.U. Gorr, C. Aparicio, Antimicrobial GL13K peptide coatings killed and ruptured the wall of streptococcus gordonii and prevented formation and growth of biofilms, PloS One 9 (2014), https://doi.org/10.1371/journal.pone.0111579 e111579.
[35] K.V. Holmberg, M. Abdolhosseini, Y. Li, X. Chen, S.U. Gorr, C. Aparicio, Bio-inspired stable antimicrobial peptide coatings for dental applications, Acta Biomater. 9 (2013) 8224–8231, https://doi.org/10.1016/j.actbio.2013.06.017.
[36] S.K. Boda, Y. Almoshari, H. Wang, X. Wang, R.A. Reinhardt, B. Duan, D. Wang, J. Xie, Mineralized nanofiber segments coupled with calcium-binding BMP-2 peptides for alveolar bone regeneration, Acta Biomater. 85 (2019) 282–293, https://doi.org/10.1016/j.actbio.2018.12.051.
[37] C.Y. Loo, D.A. Corliss, N. Ganeshkumar, Streptococcus gordonii biofilm formation: identification of genes that code for biofilm phenotypes, J. Bacteriol. 182 (2000) 1374–1382, https://doi.org/10.1128/JB.182.5.1374-1382.2000.
[38] J.B. Kaper, J.P. Nataro, H.L.T. Mobley, Pathogenic Escherichia coli, Nat. Rev. Microbiol. 2 (2004) 123–140, https://doi.org/10.1038/nrmicro818.
[39] A. Bigi, A. Ripamonti, G. Cojazzi, G. Pizzuto, N. Roveri, M.H.J. Koch, Structural analysis of Turkey tendon collagen upon removal of the inorganic phase, Int. J. Biol. Macromol. 13 (1991) 110–114, https://doi.org/10.1016/0141-8130(91)90058-3.
[40] R.E. Abouzeid, R. Khiari, D. Beneventi, A. Dufresne, Biomimetic mineralization of three-dimensional printed alginate/TEMPO-oxidized cellulose nanofibril scaffolds for bone tissue engineering, Biomacromolecules 19 (2018) 4442–4452, https://doi.org/10.1021/acs.biomac.8b01325.
[41] R. Shah, N. Saha, T. Kitano, P. Saha, Preparation of CaCO3-based biomineralized polyvinylpyrrolidone-carboxymethylcellulose hydrogels and their viscoelastic behavior, J. Appl. Polym. Sci. 131 (2014), https://doi.org/10.1002/app.40237, 40237.
[42] K.W. Kolewe, J. Zhu, N.R. Mako, S.S. Nonnenmann, J.D. Schiffman, Bacterial adhesion is affected by the thickness and stiffness of poly(ethylene glycol) hydrogels, ACS Appl. Mater. Interfaces 10 (2018) 2275–2281, https://doi.org/10.1021/acsami.7b12145.
[43] I. Mutreja, S.L. Warring, K.S. Lim, T. Swadi, K. Clinch, J.M. Mason, C.R. Sheen, D. R. Thompson, R.G. Ducati, S.T. Chambers, G.B. Evans, M.L. Gerth, A.G. Miller, T.B. F. Woodfield, Biofilm inhibition via delivery of novel methylthioadenosine nucleosidase inhibitors from PVA-tyramine hydrogels while supporting mesenchymal stromal cell viability, ACS Biomater. Sci. Eng. 5 (2019) 748–758, https://doi.org/10.1021/acsbiomaterials.8b01141.
[44] S. Acosta, L. Quintanilla, M. Alonso, C. Aparicio, J.C. Rodríguez-Cabello, Recombinant AMP/polypeptide self-assembled monolayers with synergistic antimicrobial properties for bacterial strains of medical relevance, ACS Biomater. Sci. Eng. 5 (2019) 4708–4716, https://doi.org/10.1021/acsbiomaterials.9b00247.
[45] S.U. Gorr, C.M. Flory, R.J. Schumacher, In vivo activity and low toxicity of the second-generation antimicrobial peptide DGL13K, PloS One 14 (2019), https://doi.org/10.1371/journal.pone.0216669 e0216669.
[46] H. Hirt, J.W. Hall, E. Larson, S.U. Gorr, A D-enantiomer of the antimicrobial peptide GL13K evades antimicrobial resistance in the Gram positive bacteria Enterococcus faecalis and Streptococcus gordonii, PloS One 13 (2018), https://doi.org/10.1371/journal.pone.0194900 e0194900.
[47] N.G. Fischer, D.G. Moussa, E.P. Skoe, D.A. De Jong, C. Aparicio, Keratinocyte-specific peptides-based surfaces for hemidesmosome upregulation and prevention of bacterial colonization, ACS Biomater. Sci. Eng. (2020), https://doi.org/10.1021/acsbiomaterials.0c00845.
[48] T. Li, N. Wang, S. Chen, R. Lu, H. Li, Z. Zhang, Antibacterial activity and cytocompatibility of an implant coating consisting of TiO2 nanotubes combined with a GL13K antimicrobial peptide, Int. J. Nanomed. 12 (2017) 2995–3007, https://doi.org/10.2147/IJN.S128775.
[49] Z. Ye, X. Zhu, S. Acosta, D. Kumar, T. Sang, C. Aparicio, Self-assembly dynamics and antimicrobial activity of all l- and d-amino acid enantiomers of a designer peptide, Nanoscale 11 (2019) 266–275, https://doi.org/10.1039/c8nr07334a.
[50] B. Bechinger, S.U. Gorr, Antimicrobial peptides: mechanisms of action and resistance, J. Dent. Res. (2017), https://doi.org/10.1177/0022034516679973.
[51] P.V. Giannoudis, O. Faour, T. Goff, N. Kanakaris, R. Dimitriou, Masquelet technique for the treatment of bone defects: tips-tricks and future directions, Injury 42 (2011) 591–598, https://doi.org/10.1016/j.injury.2011.03.036.
[52] Z. Ye, C. Aparicio, Modulation of supramolecular self-assembly of an antimicrobial designer peptide by single amino acid substitution: implications on peptide activity, Nanoscale Adv 1 (2019) 4679–4682, https://doi.org/10.1039/c9na00498j.
[53] Z. Ye, A. Kobe, T. Sang, C. Aparicio, Unraveling dominant surface physicochemistry to build antimicrobial peptide coatings with supramolecular amphiphiles, Nanoscale (2020), https://doi.org/10.1039/D0NR04526H.
[54] D.F. Williams, Biodegradation of surgical polymers, J. Mater. Sci. 17 (1982) 1233–1246, https://doi.org/10.1007/BF00752233.
[55] M.K.Y. Rao, P. Somasundaran, K.M. Schilling, B. Carson, K. P. Ananthapadmanabhan, Bacterial adhesion onto apatite minerals -electrokinetic aspects, Colloids Surfaces A Physicochem. Eng. Asp. 79 (1993) 293–300, https://doi.org/10.1016/0927-7757(93)80182-E.
[56] X. Chen, X.C. Zhou, S. Liu, R.F. Wu, C. Aparicio, J.Y. Wu, In vivo osseointegration of dental implants with an antimicrobial peptide coating, J. Mater. Sci. Mater. Med. 28 (2017) 76, https://doi.org/10.1007/s10856-017-5885-8.
[57] A.J. Lausch, L.C. Chong, H. Uludag, E.D. Sone, Multiphasic collagen scaffolds for engineered tissue interfaces, Adv. Funct. Mater. 28 (2018), https://doi.org/10.1002/adfm.201804730, 1804730.
[58] Y. Li, J.C. Rodriguez-Cabello, C. Aparicio, Intrafibrillar mineralization of self-assembled elastin-like recombinamer fibrils, ACS Appl. Mater. Interfaces 9 (2017) 5838–5846, https://doi.org/10.1021/acsami.6b15285.
[59] Y. Qi, Z. Cheng, Z. Ye, H. Zhu, C. Aparicio, Bioinspired mineralization with hydroxyapatite and hierarchical naturally aligned nanofibrillar cellulose, ACS Appl. Mater. Interfaces 11 (2019) 27598–27604, https://doi.org/10.1021/acsami.9b09443.
[60] Y. Qi, S. Mai, Z. Ye, C. Aparicio, Biomimetic fabrication and characterization of collagen/strontium hydroxyapatite nanocomposite, Mater. Lett. 274 (2020), https://doi.org/10.1016/j.matlet.2020.127982, 127982.
[61] K. Sariibrahimoglu, W. Yang, S.C.G. Leeuwenburgh, F. Yang, J.G.C. Wolke, Y. Zuo, Y. Li, J.A. Jansen, Development of porous polyurethane/strontium-substituted hydroxyapatite composites for bone regeneration, J. Biomed. Mater. Res. - Part A. 103 (2015) 1930–1939, https://doi.org/10.1002/jbm.a.35327.
[62] S. Chen, Y. Shi, X. Zhang, J. Ma, Biomimetic synthesis of Mg-substituted hydroxyapatite nanocomposites and three-dimensional printing of composite scaffolds for bone regeneration, J. Biomed. Mater. Res. - Part A. 107 (2019) 2512–2521, https://doi.org/10.1002/jbm.a.36757.